Supporting Information

You et al. 10.1073/pnas.1504354112

SI Materials and Methods

Reagents and Equipment. Unless otherwise stated, all reagents were purchased from Sigma-Aldrich. Commercially available reagents were used without further purification. Pyrithiamine pyrophosphate was prepared as reported previously (1). Absorbance spectra were recorded with a Thermo Scientific NanoDrop 2000 spectrophotometer with cuvette capability. Fluorescence emission and kinetics spectra were measured with a Horiba Fluoromax-4C fluorescence spectrometer. HPLC assays were performed on an Agilent 1100 series HPLC with a Zorbax C8 column (4.6 × 150 mm, 5-μm particle size). In-gel fluorescence imaging was recorded using a ChemiDoc MP imager (Bio-Rad).

Preparation of RNA Sensors and Mutants. Secondary structure prediction was performed using Mfold online software (2). Mutated and truncated RNAs were prepared by in vitro transcription using single-stranded DNA templates (Protein and Nucleic Acid Facility, Stanford University Medical Center, Stanford, CA) containing the desired mutations or truncations. Templates were PCR-amplified to create dsDNA templates using primers which included a 5′ T7 promoter sequence as described previously (3). Purified PCR products were used as templates for in vitro T7 transcription (Epicentre).

Dose–Response Curve Measurements. All in vitro RNA properties were measured in 40 mM Hepes (pH 7.4), 125 mM KCl, and 5 mM $MgCl_2$ buffer unless specified. All values presented are the average of at least three independent experiments; error bars indicate SEM value. Dose–response curves for each sensor in response to the target metabolite were determined by measuring the increase in fluorescence as a function of increasing target concentration in the presence of a fixed concentration of RNA sensor (100 nM) and a fixed concentration of fluorophore (10 μM). Fluorescence emission was recorded using the following instrument parameters: excitation wavelength, 470 nm; emission wavelength, 503 nm; slit widths, 5 nm. Curves were determined using a nonlinear regression analysis in GraphPad Prism software and matched by least squares fitting to a standard dose–response model for a 1:1 complex.

Spinach Riboswitch Activation and Deactivation Rates. To measure the activation rate, a solution of RNA sensor (100 nM) and DFHBI (10 μM) was incubated with continuous stirring at 25 °C. Then TPP (30 μM) was added rapidly to the stirring solutions, and fluorescence emission was recorded over a 25-min period under continuous illumination at 25 °C using the following instrument parameters: excitation wavelength, 470 nm; emission wavelength, 503 nm; increment of data point collection, 5 s; slit widths, 5 nm. The fluorescence increase was plotted against exposure time and normalized to the maximum intensity.

To measure the deactivation rate, a solution of RNA sensor (100 nM) and DFHBI (10 μM) was incubated with target TPP (1 mM) at 25 °C When the sensor reached the maximal fluorescence, the solution was transferred to a RNase-free Micro Bio-Spin column (Bio-Rad) containing Bio-Gel P-30. This column was buffer-exchanged with the above buffer without TPP and spun at 1,000 × *g* for 3 min. The flowthrough after gel filtration contains the sensor in a TPP-free buffer. The fluorescence emission kinetics of the flowthrough was recorded immediately over a 15-min period at 25 °C using the following instrument parameters: excitation wavelength, 470 nm; emission wavelength, 503 nm; increment of data point collection, 5 s; slit widths, 5 nm. The fluorescence decrease was plotted against time and normalized to the maximum intensity of the sensor spun through a column containing 1 mM TPP. The control experiment (buffer-exchanged columns with buffer containing the metabolite) was performed at the same time. The fluorescence of the control sample was not affected significantly by the spin and incubation process.

HPLC Measurement of Aggregate TPP Levels. Cells transformed with Spinach riboswitch were grown overnight in LB-Kan. Cultures then were diluted to OD_{600} = 0.1 in 100 mL LB-Kan and grown to OD_{600} = 0.4. Cells were induced for 2 h with 1 mM IPTG at 37 °C with constant shaking. The entire culture was centrifuged for 2 min at 5,000 × *g*. Pellets were resuspended and washed once with M9 medium and then were resuspended in 300 mL of M9 medium containing 200 μM DFHBI and were divided into three samples for replicates. After 45-min incubation at 37 °C and 1-h incubation at 25 °C, thiamine (10 μM), alone or with 1 mM oxythiamine as competitor, or vehicle alone was added to each sample, and cultures were incubated at 25 °C. Fifteen-milliliter aliquots were removed from replicated samples at each time point, centrifuged for 2 min at 5,000 × *g*, and flash frozen in liquid nitrogen. Cells were thawed on ice and lysed by resuspending the pellet in 500 μL of cold 4% perchloric acid. Insoluble material was pelleted by spinning at 5,000 × *g* for 2 min, and the supernatant was added with final concentration of 2 mM $K_3[Fe(CN)_6]$ in 0.56 M NaOH solution for oxidation. The solution was transferred to a dialysis spin column with a 10,000 molecular weight cut off (Amicon) and spun at 10,000 × *g* for 10 min at 4 °C. Then a portion of the flowthrough (50 μL) was injected on a Zorbax C8 column (Agilent) on an Agilent 1100 HPLC. Samples were loaded and eluted for 15 min with an aqueous buffer A containing 12% methanol, 1.5% *N*,*N*-dimethylformamide, 140 mM K_2HPO_4, and 0.3 mM tetrabutylammonium hydroxide, which was brought to pH 7.0 with phosphoric acid. After each sample was eluted, the column was washed with a gradient of 0–20% buffer B (70% methanol in water) for 10 min before the next sample was injected. The fluorescence emission signal was monitored at 454 nm with excitation at 360 nm. TPP standards were used to calibrate TPP levels measured using this assay.

In-Gel Spinach Riboswitch Imaging. Typically 10–200 ng of in vitro-transcribed RNA was loaded into a well of precast 6% TBE-Urea Gel (Life Technologies) and was run at 270 V in 1× Tris/borate/EDTA (TBE) buffer. RiboRuler Low Range RNA Ladder (Thermo Scientific) was used as a molecular-weight size standard. After the gel was run to completion, it was washed three times with water (5 min each washing) and then was stained for 30 min in 10 μM DFHBI in buffer containing 40 mM Hepes (pH 7.4), 125 mM KCl, 5 mM $MgCl_2$, and 100 μM TPP. Then the gel was imaged using a ChemiDoc MP (Bio-Rad) with 470/30 nm excitation and 532/28 nm emission. Next, to see all the RNA in the sample, the gel was washed again three times with water (5 min each washing) followed by staining for 30 min with SYBR Gold dye (Life Technologies) diluted 1/10,000 in TBE buffer. Then the gel was imaged under the same instrument using the preset SYBR Gold channel (302 nm excitation and 590/110 nm emission). Gel bands intensities were quantified in Image Lab 5.0 software (Bio-Rad).

1. Sudarsan N, Cohen-Chalamish S, Nakamura S, Emilsson GM, Breaker RR (2005) Thiamine pyrophosphate riboswitches are targets for the antimicrobial compound pyrithiamine. *Chem Biol* 12(12):1325–1335.
2. Zuker M (2003) Mfold web server for nucleic acid folding and hybridization prediction. *Nucleic Acids Res* 31(13):3406–3415.
3. Paige JS, Wu KY, Jaffrey SR (2011) RNA mimics of green fluorescent protein. *Science* 333(6042):642–646.

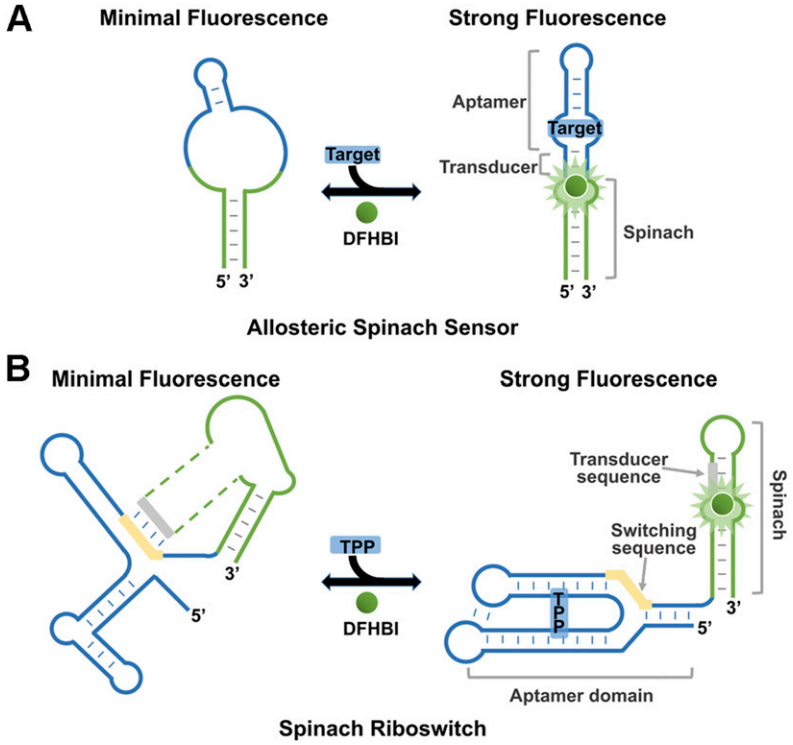

Fig. S1. The mechanism of Spinach riboswitches is different from that the allosteric Spinach sensors. (*A*) Secondary structure and design of allosteric Spinach sensors. The allosteric Spinach sensors were described previously (1) and have been used for a variety of different target molecules (1–4). The term "allosteric" is used in analogy to the metabolite-regulated allosteric ribozymes, which comprise aptamers fused to ribozymes (5). These sensors comprise two domains: Spinach (green) and a target-binding aptamer (blue). The target-binding aptamer is inserted into a structurally critical helix of Spinach (1). The target-binding aptamer is unstructured without the target molecule. However, when the aptamer binds its target, the aptamer folds, enabling the folding of the critical helix in Spinach, and allows Spinach to bind and activate the fluorescence of DFHBI (green ball). (*B*) Secondary structure and design of Spinach riboswitch. The Spinach riboswitch uses a sensing mechanism that is fundamentally different from that of the allosteric Spinach sensor. The Spinach riboswitch is generated by swapping Spinach (green) into the expression platform of riboswitch. The transducer sequence (gray) is released from the switching sequence (yellow) in the aptamer domain, forming a critical helix in Spinach. Formation of the helix is critical for Spinach to bind and activate the fluorescence of DFHBI (green ball).

1. Paige JS, Nguyen-Duc T, Song W, Jaffrey SR (2012) Fluorescence imaging of cellular metabolites with RNA. *Science* 335(6073):1194.
2. Song W, Strack RL, Jaffrey SR (2013) Imaging bacterial protein expression using genetically encoded RNA sensors. *Nat Methods* 10(9):873–875.
3. Kellenberger CA, Wilson SC, Sales-Lee J, Hammond MC (2013) RNA-based fluorescent biosensors for live cell imaging of second messengers cyclic di-GMP and cyclic AMP-GMP. *J Am Chem Soc* 135(13):4906–4909.
4. Kellenberger CA, Hammond MC (2015) In vitro analysis of riboswitch-Spinach aptamer fusions as metabolite-sensing fluorescent biosensors. *Methods Enzymol* 550:147–172.
5. Tang J, Breaker RR (1997) Rational design of allosteric ribozymes. *Chem Biol* 4(6):453–459.

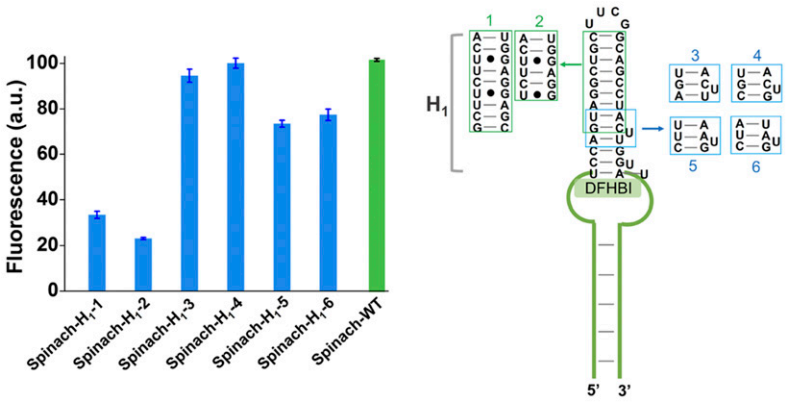

Fig. S2. Effect of different H_1 sequences on Spinach fluorescence signals. In Fig. 2*A*, we changed the helical sequence (H_1 helix) above the DFHBI-binding pocket. In each helix, one of the strands constitutes the transducer sequence that is tested in Fig. 2*A*. However, it is possible that these changes impair Spinach fluorescence. This experiment was performed to determine if the different fluorescence signals seen in the six transducer sequence-variant Spinach riboswitches (transducers 1–6 in Fig. 2*A*) are caused by impaired folding and fluorescence of the Spinach–DFHBI complex. This experiment is important because the H_1 sequence region adjacent to the DFHBI-binding pocket is known to have a structural role in Spinach-induced DFHBI fluorescence (1). Thus, we tested each of the variants in Spinach alone (Spinach-H_1-1–6), i.e., without the rest of the riboswitch present. (The numbers 1–6 within these variants' names represent the corresponding transducer number in Fig. 2*A*.) Spinach-H_1-3 has the same H_1 helix sequence as the wild-type Spinach (Spinach-WT). The green box highlights the H_1 sequence mutations in Spinach-H_1-1 and Spinach-H_1-2 compared with Spinach-H_1-3, and the blue box highlights the corresponding H_1 sequence mutations in Spinach-H_1-4–Spinach-H_1-6. Spectra were collected by mixing 100 nM RNA with 10 μM DFHBI. Shown are mean and SEM values of three independent replicates.

1. Paige JS, Nguyen-Duc T, Song W, Jaffrey SR (2012) Fluorescence imaging of cellular metabolites with RNA. *Science* 335(6073):1194.

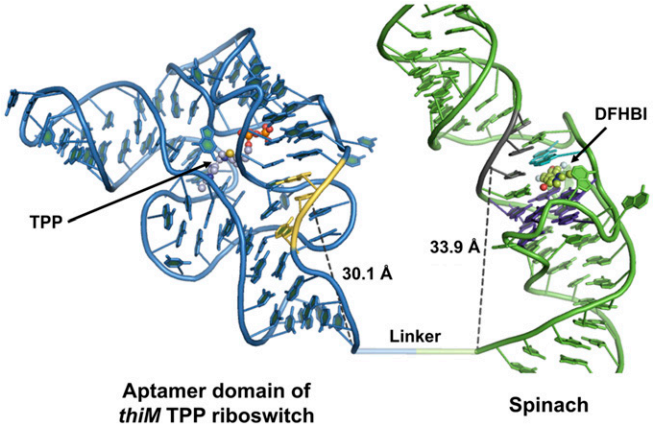

Fig. S3. Structural model of the optimal Spinach riboswitch. In this figure, we examine how the transducer sequence (gray) in the Spinach part of the Spinach riboswitch is positioned in space relative to the switching sequence (yellow). Thus, we prepared a structural model of the Spinach riboswitch using linker 3 from Fig. 2*B*. This linker shows the best signal-to-noise behavior in the in vitro assay (Fig. 2*B*). In the model shown here, the blue chain indicates the aptamer domain of the *E. coli thiM* riboswitch (1), and the green chain indicates the Spinach sequence (2) that is used in the optimal Spinach riboswitch. TPP and DFHBI are highlighted in a ball-and-stick model with the oxygen element in red, the phosphate element in gold, the sulfur element in yellow, and DFHBI backbone elements in green. In this model, the predicted distance from the linker connection point with Spinach to the switching sequence (~30.1 Å) is nearly the same as the distance to the corresponding U base of transducer sequence in Spinach (~33.9 Å). This structural model of the optimal Spinach riboswitch suggests that the position of the transducer sequence allows it to interact readily with the switching sequence in the riboswitch. Thus, the improved performance of linker 3 may reflect optimized positioning of the transducer sequence relative to the switching sequence.

1. Edwards TE, Ferré-D'Amaré AR (2006) Crystal structures of the thi-box riboswitch bound to thiamine pyrophosphate analogs reveal adaptive RNA-small molecule recognition. *Structure* 14(9):1459–1468.
2. Warner KD, et al. (2014) Structural basis for activity of highly efficient RNA mimics of green fluorescent protein. *Nat Struct Mol Biol* 21(8):658–663.

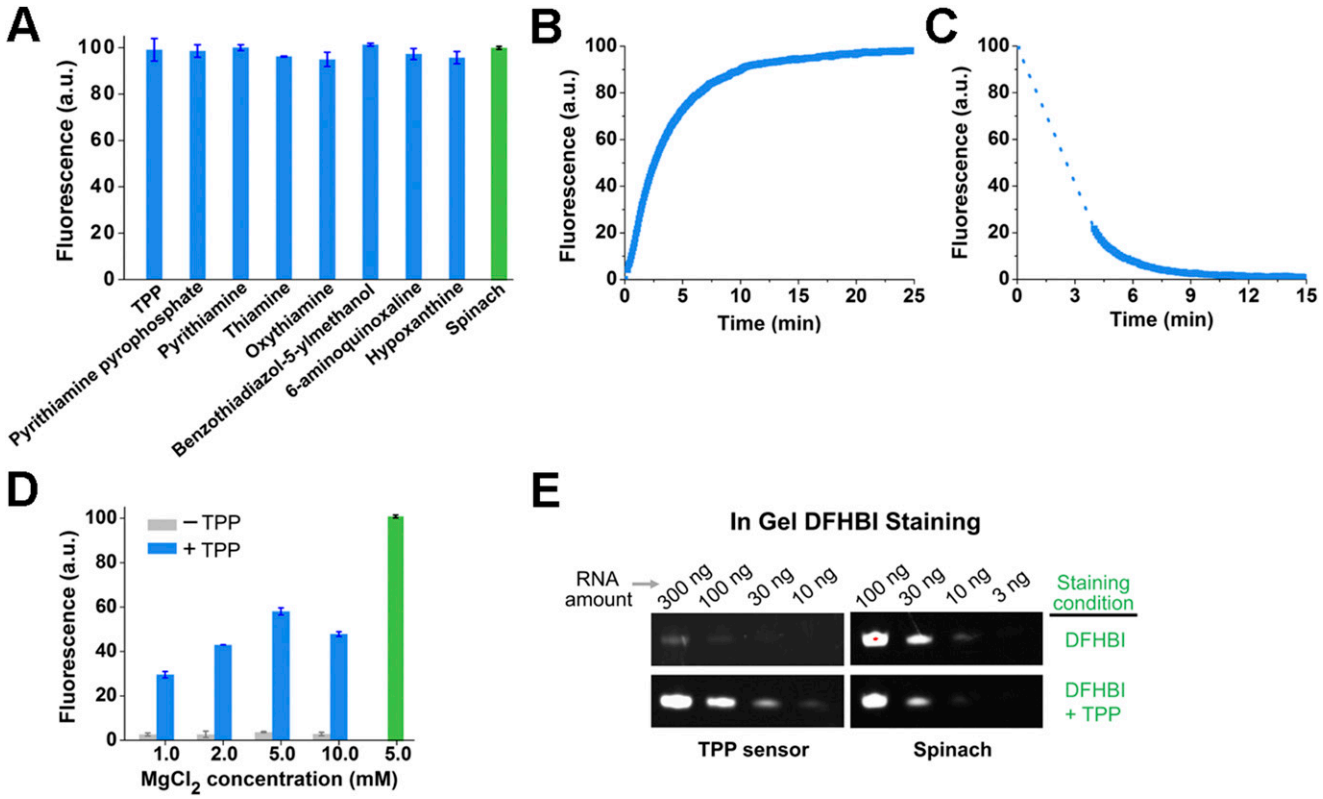

Fig. S4. In vitro properties of the optimized Spinach riboswitch. (*A*) The effect of different compounds on Spinach fluorescence. In several of our experiments, we added compounds to the Spinach riboswitch and observed little or no fluorescence. For example, in Fig. 3*D*, thiamine, pyrithiamine, and oxythiamine induced nearly undetectable levels of fluorescence in the TPP Spinach riboswitch. In Fig. 4, the Spinach riboswitch was used to identify antagonists and agonists of the TPP riboswitch. It is remotely possible that the compounds inhibit the Spinach portion of the sensor, perhaps by competing with DFHBI or by unfolding Spinach. To see if the compounds have any effect on Spinach fluorescence, we incubated oxythiamine, pyrithiamine, pyrithiamine pyrophosphate, hypoxanthine, 6-aminoquinoxaline, and benzothiadiazol-5-ylmethanol with Spinach. None of these compounds had a substantial effect on Spinach fluorescence. Spectra were collected by mixing 100 nM Spinach with 10 μM DFHBI and 100 μM each compound. Shown are mean and SEM values of three independent replicates. (*B*) Measurement of the rate of Spinach riboswitch activation. The addition of TPP led to rapid signal acquisition, with more than half of the total fluorescence signal appearing in 150 s and with maximal levels reached within ~10 min. (*C*) To determine how quickly Spinach riboswitch fluorescence is lost once TPP is removed from the sensor, we used a gel filtration spin column (Bio-Rad) to remove the TPP. Spinach riboswitch fluorescence was deactivated by >90% within 8 min. (Because the spin column was centrifuged for 3 min, fluorescence measurements cannot be made for the first 3 min.) (*D*) Measurement of magnesium-dependent fluorescence of the Spinach riboswitch. The TPP riboswitch has magnesium-dependent binding to TPP, and different studies have examined TPP riboswitch behavior at different magnesium concentrations. Thus, we wanted to present measurements at the magnesium concentrations commonly used in the literature for this riboswitch. In these experiments, 100 nM RNA was mixed with 10 μM DFHBI and 100 μM TPP, and the fluorescence signal of the complex was measured at the indicated concentrations of $MgCl_2$. As a control, Spinach fluorescence (green) was measured at 5 mM $MgCl_2$ under the same experimental conditions. Shown are mean and SEM values of three independent replicates. (*E*) We recently developed an in-gel imaging method to quantify intracellular Spinach levels by staining gels with DFHBI (1). To determine if this method can be used to determine a TPP-dependent activation of Spinach riboswitch fluorescence, we prepared a serial dilution of in vitro-transcribed Spinach riboswitch and Spinach. The RNA was resolved by a 6% urea-PAGE gel followed by staining with 10 μM DFHBI in the absence or presence of 100 μM TPP. In these experiments, the Spinach riboswitch is not seen in DFHBI-stained gels, presumably because the Spinach region is not folded. However, a clear Spinach riboswitch band is seen when the gel is soaked with both DFHBI (10 μM) and TPP (100 μM). Exposure time, 3 s. This experiment further demonstrates that the Spinach riboswitch undergoes a TPP-dependent activation of Spinach fluorescence.

1. Filonov GS, Moon JD, Svensen N, Jaffrey SR (2014) Broccoli: Rapid selection of an RNA mimic of green fluorescent protein by fluorescence-based selection and directed evolution. *J Am Chem Soc* 136(46):16299–16308.

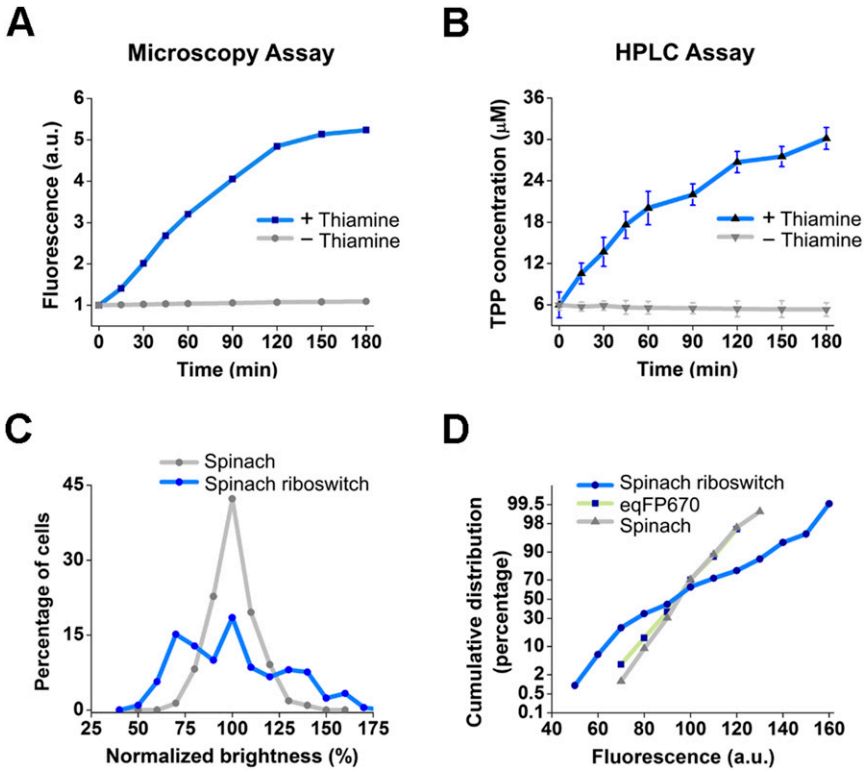

Fig. S5. The Spinach riboswitch measures TPP biosynthesis rates in living cells. (*A* and *B*) The fluorescence seen in cells (*A*) and the absolute TPP levels as measured using an HPLC assay (*B*). We wanted to know how the intracellular fluorescence levels correlate with the TPP levels and if linear increases in intracellular TPP levels correlate with linear increases in Spinach riboswitch fluorescence. First, we monitored Spinach riboswitch fluorescence after the addition of thiamine (10 μM). Cells expressing the Spinach riboswitch were thiamine starved briefly, and the fluorescence level in single living cells was measured by epifluorescence microscopy every 15 min following 10 μM thiamine treatment and was plotted as shown in *A*. The mean fluorescence was calculated from 250 cells at each time point over three experimental replicates. Next, we measured the actual TPP levels in cells. Cells treated identically were lysed at different time points to measure total TPP levels using an HPLC assay and were plotted in *B*. The linear increase in TPP levels corresponds with a similar increase in Spinach riboswitch fluorescence. Thus, the sensor shows linear fluorescence over the indicated range of cellular TPP concentration. Error bars represent the SEM from three experimental replicates. (*C*) In this experiment, we wanted to understand the variability in Spinach riboswitch fluorescence after thiamine treatment. In Fig. 5*C* we showed that the cell-to-cell variability in Spinach riboswitch fluorescence is greater than the cell-to-cell variability in eqFP670 fluorescence, suggesting that the variability in cell-to-cell Spinach riboswitch fluorescence is not caused by variable expression levels. However, here we did another control. We used the same expression plasmid and expressed Spinach instead of the Spinach riboswitch. We then monitored the variability in Spinach fluorescence after thiamine treatment. *E. coli* cells were imaged at 3 h after treatment with 10 μM thiamine. The average fluorescence value was set to 100%, and individual cells were binned according to relative brightness. The percentage of cells in each bin was plotted. A total of 250 cells were quantified from three experimental replicates. As can be seen, Spinach itself shows much less cell-to-cell variation than Spinach riboswitch fluorescence. These data suggest that the variation seen in individual cells reflects variable TPP levels and is not a simple artifact of Spinach riboswitch expression levels. (*D*) Cumulative percentage frequency distribution plots to test for non-Gaussian distribution. We asked if the Spinach riboswitch fluorescence variation seen in cells follows a Gaussian or non-Gaussian distribution. A non-Gaussian distribution would be expected if particular cells are outliers with unusually high or low TPP levels. Fluorescence values were tabulated as percentages and plotted on a cumulative probability axis. A linear curve would indicate sampling from a Gaussian/normal distribution, as observed for the Spinach and eqFP670 distributions. Deviation from linearity implies nonnormality, as observed in the Spinach riboswitch.

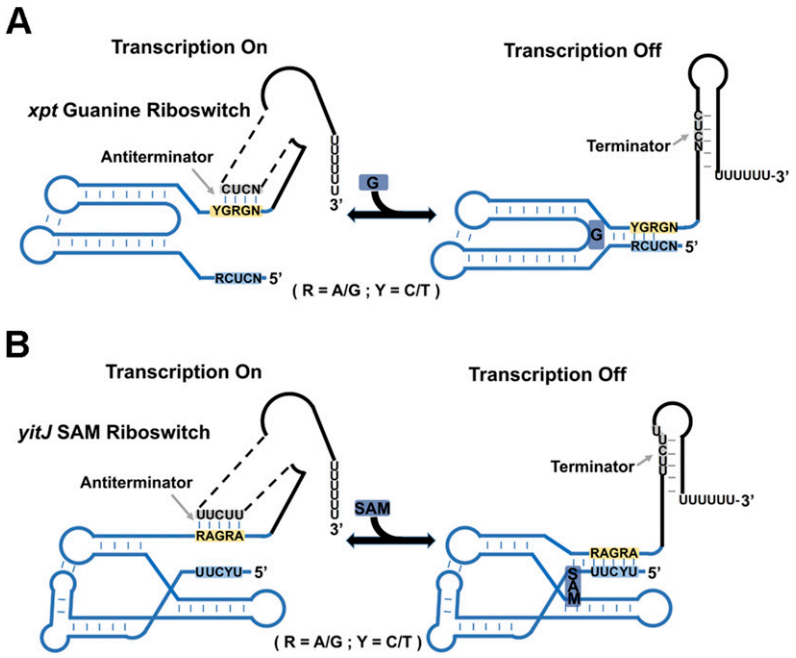

Fig. S6. Natural transcription control mechanism of the *xpt* purine and the *yitJ* SAM-I riboswitches. (*A*) Purine-dependent transcription control mechanism of the *xpt* riboswitches. The guanine binding by the aptamer domain (blue) induces a predictable structural switch in the expression platform (black). The relative binding affinity between the switching sequence (yellow) and the competitor sequence of aptamer domain (blue) or the transducer sequence of expression platform (gray) is tuned by purine binding. (*B*) SAM-dependent transcription control mechanism of the *yitJ* SAM-I riboswitches. SAM binding by the aptamer domain (blue) induces a well-defined structural switch in the expression platform (black). The relative binding affinity between the switching sequence (yellow) and the competitor sequence of aptamer domain (blue) or the transducer sequence of expression platform (gray) is tuned by SAM binding.

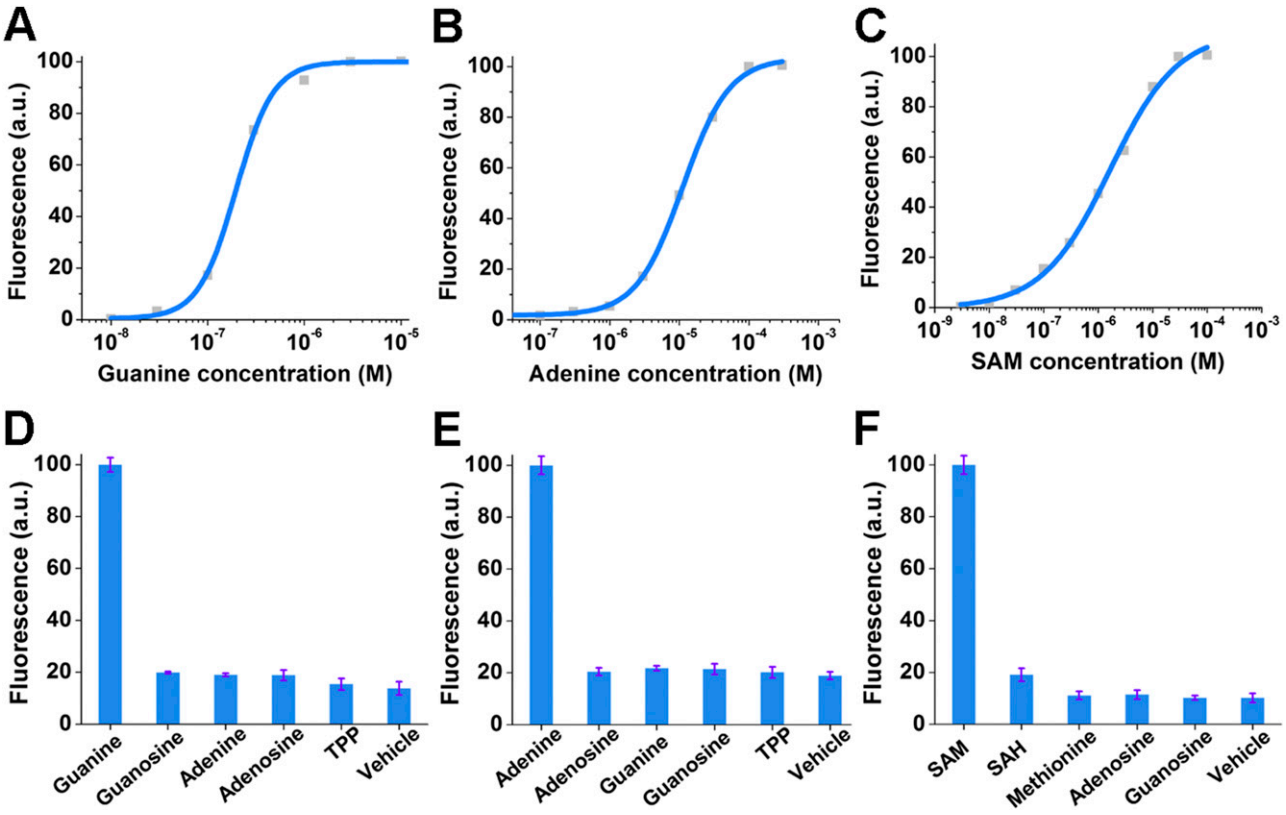

Fig. S7. Sensitivity and selectivity of the Spinach riboswitches. (*A*) Dose–response curve for fluorescence detection of guanine by the guanine Spinach riboswitch. Half-maximal fluorescence is reached at 190 nM guanine. (*B*) Dose–response curve for fluorescence detection of adenine by the adenine Spinach riboswitch. Half-maximal fluorescence is reached at 10 μM adenine. (*C*) Dose–response curve for fluorescence detection of SAM by the SAM-I Spinach riboswitch. Half-maximal fluorescence is reached at 1.2 μM SAM. (*D*) Selectivity of the guanine Spinach riboswitch. Fluorescence emission was measured in the presence of 10 μM guanine or competing metabolites. Shown are mean and SEM values of three independent replicates. (*E*) Selectivity of the adenine Spinach riboswitch. Fluorescence emission was measured in the presence of 100 μM adenine or competing metabolites. Shown are mean and SEM values of three independent replicates. (*F*) Selectivity of the SAM-I Spinach riboswitch. Fluorescence emission was measured in the presence of 10 μM SAM or competing metabolites. Shown are mean and SEM values of three independent replicates.

Table S1. Sequences for the Spinach riboswitches

Target metabolite	RNA sensor sequence
TPP	GACUCGGGGUGCCCUUGUGCGUCAAGGCUGAGAAAAUACCCGUAUCACCUGAUCUGGAUAAUG-CCAGCGUAGGGAAGUCACAUGGUGAAGGACGGGUCCCGUAGGCUGCUUCGGCAGCCUACU-GGUUGAGUAGAGUGUGAGCUCCGU
Guanine	GAACUCAUAUAAUCGCGUGGAUAUGGCACGCAAGUUUCUACCGGGCACCGUAAAUGUCCGACU-AUGGGAGAGCAAUGAUGGUGAAGGACGGGUCCCGCUUGCUCUUUAUUUGAGCGGGCUUGUU-GAGUAGAGUGUGAGCUCCGU
Adenine	GAAUCAUAUAAUCGCGUGGAUAUGGCACGCAAGUUUCUACCGGGCACCGUAAAUGUCCGAUUA-UGGGAGAGCAAUGAUGGUGAAGGACGGGUCCCGCUUGCUCUUUAUUUGAGCGGGCUUGUUG-AGUAGAGUGUGAGCUCCGU
SAM	GUACUCAUCAAGAGAAGCAGAGGGACUGGCCCGACGAAGCUUCAGCAACCGGUGUAAUGGCGA-UCAGCCAUGACCAAGGUGCUAAAUCCAGCAAGCUCGAACAGCUUGGAAGAUGGGAAGAGCG-UUAUGGUGAAGGACGGGUCCCGUAGGCUGCUUCGGCAGCCUACUGGUUGAGUAGAGUGUGA-GCUCCGU

The blue sequence indicates the aptamer domain of each riboswitch, and the green sequence indicates the Spinach sequence that is used in all sensors. In this article, "Spinach" designates the core DFHBI-binding domain of Spinach2 (1), as well as the proximal sequences above and below the G-quadruplex motif (2, 3). "Spinach" does not refer to the entire aptamer sequence of Spinach or Spinach2, which contains additional helical elements that are not required for fluorescence (2, 3). Highlighted yellow and gray regions indicate the switching sequence and the transducer sequence, respectively.

1. Strack RL, Disney MD, Jaffrey SR (2013) A superfolding Spinach2 reveals the dynamic nature of trinucleotide repeat-containing RNA. *Nat Methods* 10(12):1219–1224.
2. Huang H, et al. (2014) A G-quadruplex-containing RNA activates fluorescence in a GFP-like fluorophore. *Nat Chem Biol* 10(8):686–691.
3. Warner KD, et al. (2014) Structural basis for activity of highly efficient RNA mimics of green fluorescent protein. *Nat Struct Mol Biol* 21(8):658–663.